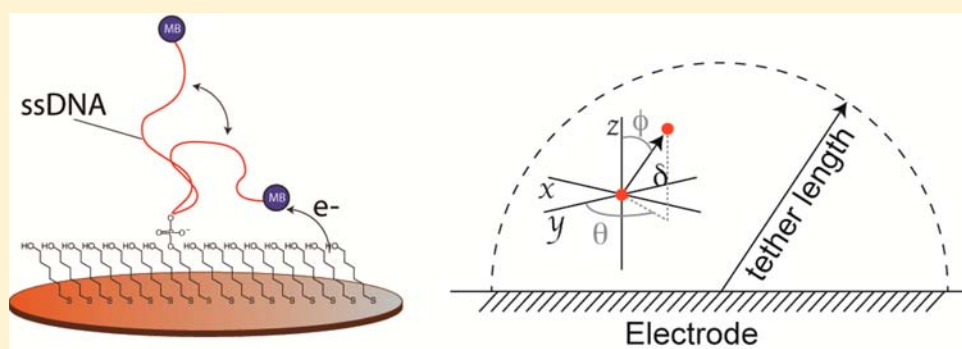


Random Walk on a Leash: A Simple Single-Molecule Diffusion Model for Surface-Tethered Redox Molecules with Flexible Linkers

Kuan-Chun Huang and Ryan J. White*

Department of Chemistry and Biochemistry, University of Maryland, Baltimore County, 1000 Hilltop Circle, Baltimore, Maryland 21250, United States

S Supporting Information



ABSTRACT: We develop a random walk model to simulate the Brownian motion and the electrochemical response of a single molecule confined to an electrode surface via a flexible molecular tether. We use our simple model, which requires no prior knowledge of the physics of the molecular tether, to predict and better understand the voltammetric response of surface-confined redox molecules when motion of the redox molecule becomes important. The single molecule is confined to a hemispherical volume with a maximum radius determined by the flexible molecular tether (5–20 nm) and is allowed to undergo true three-dimensional diffusion. Distance- and potential-dependent electron transfer probabilities are evaluated throughout the simulations to generate cyclic voltammograms of the model system. We find that at sufficiently slow cyclic voltammetric scan rates the electrochemical reaction behaves like an adsorbed redox molecule with no mass transfer limitation; thus, the peak current is proportional to the scan rate. Conversely, at faster scan rates the diffusional motion of the molecule limits the simulated peak current, which exhibits a linear dependence on the square root of the scan rate. The switch between these two limiting regimes occurs when the diffusion layer thickness, $(2Dt)^{1/2}$, is ~ 10 times the tether length. Finally, we find that our model predicts the voltammetric behavior of a redox-active methylene blue tethered to an electrode surface via short flexible single-stranded, polythymine DNAs, allowing the estimation of diffusion coefficients for the end-tethered molecule.

INTRODUCTION

The utilization of electrode-tethered redox moieties is found throughout many fields and disciplines, including chemical and biosensor development,^{1–10} molecular electronics,^{11–13} and the molecular storage of energy^{14–16} and data.^{17–19} In each of these examples, a redox-active molecule is placed within nanometers of either an electrode surface or other redox molecules. In the limit of no diffusional motion of the redox molecules, the electron transfer rate is expected to be exponentially dependent on the distance (r) from the electrode surface, with the decay rate determined by a tunneling factor ($\beta = \sim 1 \text{ \AA}^{-1}$)²⁰ through the following relationship:

$$k(r)_{\text{ET}} = k_{\text{ET}}^{\circ} e^{-\beta r} \quad (1)$$

In eq 1, $k(r)_{\text{ET}}$ is the distance-dependent first-order rate constant (s^{-1}) and k_{ET}° is the standard first-order rate constant (s^{-1}) at the surface of the electrode ($r = 0$). Smalley et al.²¹ and Finklae et al.²⁰ have demonstrated that electron transfer rates for redox moieties attached to monolayers of alkanethiols

adhere to this model. They achieve this by controlling the distance between the redox molecule and the electrode surface using tightly packed alkanethiol monolayers of varying numbers of carbon atoms. To observe the exponential relationship described by eq 1, the self-assembled monolayer (SAM) must be free of defects and tightly packed, ensuring no motion of the redox molecule.^{20,21}

A very different current response is observed when the tethered redox molecules are not statically confined to the electrode surface. This occurs when short-range motions of the redox molecule become a significant contributor to the observed current of the system.^{22–28} For example, Amatore, Maisonhaute, and co-workers observed a deviation from the electron transfer rate predicted by eq 1 when studying fullerodendrimers attached to gold electrode surfaces.²⁸ As dendrimer generations increased, and thus the separation

Received: June 17, 2013

Published: August 6, 2013

distance (r) between the electrode and the redox-active C_{60} , it was anticipated that electron transfer rates would follow eq 1. Instead, they observed that the rate was almost independent of the dendrimer generation as a result of tether flexibility, which allows the redox-active C_{60} to reach the surface to undergo electron transfer. The separation distance between the electrode and redox element is not fixed, and thus, the motion of the redox moiety becomes important in the electrochemical response.

Changes in flexibility in the molecular tether of a redox molecule can be, and have been, extensively exploited to develop chemical and biosensing platforms.^{4,6,9,29,30} For example, a class of DNA hybridization-based sensors involve tethering a redox molecule to an electrode surface with single-stranded DNA.^{4,31,32} In the simplest embodiment of this type of sensor, a single-stranded DNA is hybridized with its complementary target to change the flexibility of the surface-bound probe. This change in flexibility, in turn, changes the measured faradic current resulting from the reduction/oxidation of the appended redox marker.³¹ In another approach, Plaxco,⁸ Gothelf,⁶ and O'Sullivan²⁹ and co-workers all employ structure-switching oligonucleotide aptamers attached to the electrode surface that undergo a conformation and/or flexibility change when binding a specific target. This change, again, alters the electron transfer efficiency, and the resultant changes in faradic current are used to quantify a specific target. In all of these examples, the sensors require that the monolayer of the oligonucleotide is loosely packed to allow motion of the redox molecule. Sensor signaling in these types of sensors can be furthered controlled by changing the time scale of the voltammetric interrogation (i.e., scan rate, frequency, etc.), suggesting that information on the dynamics of the molecular tether is important to understand the electrochemical response of such platforms and sensor development.^{9,32}

Understanding the electrochemical response of a tethered redox molecule can provide insight into the molecular dynamics of the tethering molecule and the motion of the redox molecule. Here, we develop a single-molecule random walk model to provide a physical picture for what is occurring at the electrode surface with a tethered redox molecule and how it affects the voltammetric response of the system. The random walk model simulates the random motion of a redox molecule confined to a hemispherical volume above an electrode surface and requires no knowledge of the physics (e.g., diffusive motion) of the tethering molecule. This is because the molecular tether does not exist in the simulation other than for determining the radius of the hemisphere in which the molecule is allowed to diffuse. We incorporate electron transfer probabilities as a function of distance from the electrode surface and the applied potential on the electrode to generate voltammograms. We then demonstrate our model predicts the observed voltammetric response of a redox molecule (methylene blue) attached to short, flexible, single-stranded DNA similar to the systems described by the above-mentioned DNA-based sensors.

MATERIALS AND METHODS

Materials. Trizma base, NaCl, KCl, 6-mercapto-1-hexanol (99%), and tris(2-carboxyethyl)phosphine (Sigma-Aldrich) were all used as received. Single-stranded, polythymine DNA (Biosearch Technologies Inc., Novato, CA) purified using dual HPLC by the manufacturer was used as received. The DNA is modified at the 5'-terminus with a

hexanethiol linker (5'-d-thiol- C_6) and at the 3'-end with a redox-active methylene blue (MB). The polythymine (T) sequences used were 5'-d-thiol- C_6 -T $_n$ -MB-3', where $n = 7, 14,$ or 21 . All solutions were prepared with ultrapure water to contain 25 mM Tris buffer, 100 mM NaCl, at a pH of 7.4.

Modified Electrode Preparation. Chemically modified electrodes were prepared as previously described.³³ Briefly, 2 mm diameter polycrystalline gold electrodes (CH Instruments, Austin, TX) were cleaned by hand polishing with a 1 μ m monocrystalline diamond suspension (Buehler, Lake Bluff, IL) on a microcloth for 1 min followed by sonication in ultrapure water for 5 min. The electrodes were further cleaned by repeated oxidative and reductive scans in 0.1 M NaOH to remove any adsorbed organics. Next a series of oxidation and reduction scans were performed in both 0.5 H₂SO₄ and 0.1 M H₂SO₄/0.01 M KCl. To verify that the electrode was clean, the electrode area was examined by integration of the gold oxide reduction peak in 0.05 M H₂SO₄.³³ Prior to DNA immobilization, the DNA was treated with 10 mM tris(2-carboxyethyl)phosphine for 1 h to reduce the disulfide bonds from strand synthesis. To prepare the redox-modified electrode surface, the cleaned electrodes were immersed in a 250 nM thiolated DNA solution for 2 h. Finally, the DNA-modified electrodes were thoroughly rinsed with water before immersion into a 3 mM 6-mercapto-1-hexanol solution in Tris buffer for 24 h to remove any nonspecifically adsorbed DNA on the electrode surface.³⁴

Electrochemical Measurements. The modified electrodes were analyzed using cyclic voltammetry with a CH Instruments electrochemical workstation (660D, Austin, TX). Experiments were performed in 25 mM Tris buffer with 100 mM NaCl at a pH of 7.4. All measurements were performed in a standard three-electrode cell with a silver/silver chloride reference electrode (Ag/AgCl, 3.0 M NaCl saturated) and a platinum wire counter electrode.

Random Walk Simulation. The simulation of the random motion of a single molecule was performed using Matlab (MathWorks 2011b) similar to the model described by White and White.^{35,36} To mimic a tethered redox molecule, the random motion of the molecule is confined to a hemispherical volume above the electrode surface. The radius of this volume is determined by the molecular tether length (L) and ranged from 5 to 20 nm (Figure 1, top). To model the 3-dimensional diffusion of a redox molecule, the molecule truly steps in any direction in three dimensions similar to the recent report by Compton and co-workers.³⁷ This is achieved by randomly generating two angles (Φ and θ) from the origin (Figure 1, top) (i.e., the location of the molecule). Ultimately, the net displacement, or step length (δ), is defined by the displacement in each of the x , y , and z directions from the origin:

$$\delta = \sqrt{x^2 + y^2 + z^2} \quad (2)$$

The molecular diffusion coefficient (D) is related to the step length through the following relationship as described by Berg: $D = \delta^2/2\tau$, where D is the diffusion coefficient (cm²/s) and τ is the step time (s).³⁸

The instantaneous velocity of the molecule ($v = \delta/\tau$ (cm/s)) is used to determine δ and τ values and ultimately a diffusion coefficient. To model the motion of a relatively small molecule, we use a diffusion coefficient of 10⁻⁵ cm²/s. Using the root-mean-square velocity as $\langle v^2 \rangle^{1/2} = kT/m$, where k is the Boltzmann constant, T is temperature, and m is the mass of a single molecule (3.1 \times 10⁻²² g assuming a molar mass of 186.04 g/mol for a molecule such as ferrocene), and a diffusion coefficient of 10⁻⁵ cm²/s, we calculate a step length of 0.02 nm and a step time of 0.2 ps and use these values throughout unless otherwise noted. More information on the relationship of δ , τ , and D can be found in refs 35 and 38.

To begin the random walk, the redox molecule starts at a random position in the confined volume and is allowed to step for N steps (typically between 10⁵ and 10⁷ steps). During the diffusion process, when the molecule reaches the outer boundary position determined by the tether length (Figure 1, top), it undergoes an elastic collision, or is reflected, for computational simplicity. Similarly, the molecule is reflected off of the electrode surface ($z = 0$) in the event of a collision.

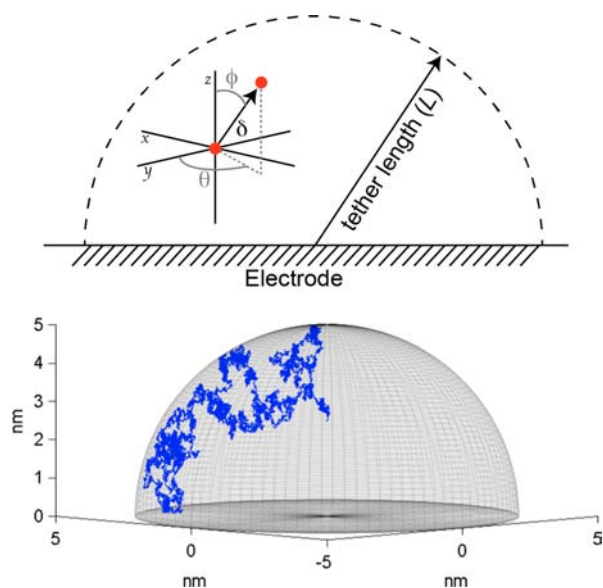


Figure 1. (Top) The simulation geometry confines the random motion of a molecule to a hemispherical volume about an electrode with a radius determined by the molecular tether length (L). The molecule is allowed to step in any 3-dimensional direction determined by two angles (Φ and θ) that are randomly generated. (Bottom) The simulated trajectory of a single molecule follows Brownian motion. In this simulation, a molecule with a 5 nm tether took 10^5 steps, equivalent to a trajectory time of 20 ns. The molecule collided with the electrode surface 38 times and reached the end of the tether 337 times.

A representative random walk simulation of a molecule tethered to the surface via a 5 nm linker is shown in Figure 1. In this figure, the molecule took 10^5 steps equivalent to 20 ns. During the simulation, the molecule collided with the electrode surface 38 times and reached the end of the tether 337 times.

Incorporation of Electron Transfer Probabilities. To evaluate the probability that an electron transfer event would occur between the redox molecule and the electrode, we determine the distance- and potential-dependent electron transfer rate similar to previously described methods.³⁶ The reaction modeled was a reversible, one-electron oxidation of the redox molecule, Red:



In eq 3, k_{Red} and k_{Ox} are the potential- and distance-dependent rates (s^{-1}) of reduction and oxidation, respectively. These rates vary with the applied potential according to the following Butler–Volmer kinetic expressions:³⁹

$$k_{\text{Red}} = k(r)_{\text{ET}} \exp\left[\frac{-\alpha nF}{RT}(E - E^\circ)\right] \quad (4)$$

and

$$k_{\text{Ox}} = k(r)_{\text{ET}} \exp\left[\frac{(1 - \alpha)nF}{RT}(E - E^\circ)\right] \quad (5)$$

In these expressions, $k(r)_{\text{ET}}$ is the distance-dependent electron transfer rate described by eq 1, α is the transfer coefficient (0.5), E is the applied potential, and E° is the standard reduction potential of the molecule (V). Combining eqs 4 and 5 with eq 1 yields the rate expressions that are evaluated at each step of the simulation:

$$k_{\text{Red}} = (k_{\text{ET}}^\circ e^{-\beta r}) \exp\left[\frac{-\alpha nF}{RT}(E - E^\circ)\right] \quad (6)$$

and

$$k_{\text{Ox}} = (k_{\text{ET}}^\circ e^{-\beta r}) \exp\left[\frac{(1 - \alpha)nF}{RT}(E - E^\circ)\right] \quad (7)$$

To provide realistic values for our standard electron transfer rate constant (k°) and tunneling decay coefficient (β), we employ values that were experimentally determined for a relatively fast, outer-sphere electron transfer redox couple—ferrocene/ferrocenium.²¹ Smalley et al. extrapolate a standard electron transfer rate constant and tunneling decay coefficient for ferrocene via measurements of electron transfer rates of ferrocene-terminated alkanethiols of $6 \times 10^8 \text{ s}^{-1}$ and 1 \AA^{-1} , respectively.²¹ These values are used throughout the reported simulations.

The probability of an electron transfer event occurring is calculated taking into account the electron transfer rate at that point of the simulation and the time the molecule will spend at that position (τ) as previously described.³⁶ Equations 8 and 9 are used to calculate the electron transfer probability of a reduction or oxidation event, respectively. P_{Red} was evaluated if the molecule was in the oxidized state, and P_{Ox} was used if the molecule was in the reduced state.

$$P_{\text{Red}} = 1 - \exp\{-k_{\text{Red}}\tau\} \quad (8)$$

$$P_{\text{Ox}} = 1 - \exp\{-k_{\text{Ox}}\tau\} \quad (9)$$

The occurrence of an electron transfer event is evaluated at each step by comparing the electron transfer probability with a uniformly generated random number between 0 and 1 with the same amount of significant figures as the probability. If the probability is smaller than the random number generated, an electron transfer event occurs. If the electron transfer probability is greater than the randomly generated number, the transfer event does not occur.

Simulation of Cyclic Voltammograms. To model cyclic voltammograms of surface-confined redox molecules, simulations were run at varying potentials ($E - E^\circ$) ranging from -200 to $+400$ mV in 10 mV intervals. Throughout the simulation, the state of the molecule (reduced or oxidized) was tracked with the molecule beginning in the reduced state at -200 mV. The simulations were run for 100 individual redox molecules, equivalent to an electrode surface with 100, noninteracting, tethered redox molecules. The scan rate is controlled by varying the number of steps occurring at each applied potential ranging from 5×10^3 to 1×10^6 steps, which corresponds to scan rates of 10^9 to 5×10^3 V/s *vide infra*. While each potential point was simulated independently, as the potential changes, the simulation takes into account the state and the position of the molecule in the preceding potential step.

Recording information about the state of the molecule with several different applied potentials and amounts of time at each potential ultimately enables the generation of voltammograms for our theoretical system. At each potential step, the simulation is run for the specified number of steps and the status of the molecule on the last step is recorded. Tracking this allows the generation of a survival probability plot (Figure 2, top). The survival probability plot in Figure 2 shows a plot of the probability of the molecule remaining in the reduced state after 10^6 steps per potential increment. These simulations were performed using a linker length of 5 nm and a diffusion coefficient of $10^{-5} \text{ cm}^2/\text{s}$. As the potential approaches E° , the survival probability approaches ~ 0.5 . As the potential is scanned further positive, the survival probability approaches 0. In other words, as the potential approaches more positive values, the oxidation reaction becomes more favored than the reduction reaction and thus the molecule is more likely to undergo an electron transfer event from Red to Ox.

The plot of survival probability can be converted into a voltammogram, noting that current is a measure of the reaction rate and thus the change in concentration of the reduced form as a function of time ($\Delta C_{\text{Red}}/\Delta t$, where C_{Red} is the concentration of the redox molecule in the reduced form). We take the derivative of this probability curve with respect to the time of the simulation to generate voltammograms. We use voltage increments of 1 mV, as compared to the 10 mV potential steps in the simulation, to smooth the resulting voltammogram. Noting that 1 electron of charge is $1.6 \times 10^{-19} \text{ C}$, we

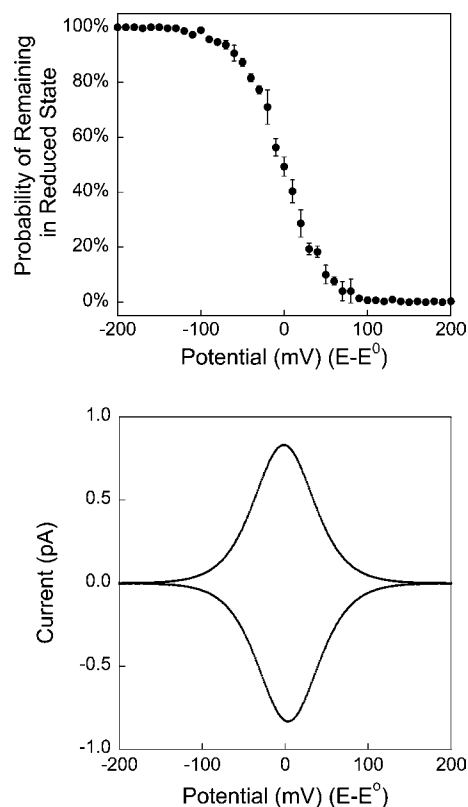


Figure 2. The survival probability of the molecule remaining in the starting reduced state is used to generate cyclic voltammograms. (Top) The probability of 100 molecules tethered via a 5 nm linker remaining in the reduced state at a slow scan rate of 5×10^3 V/s was simulated with 10^6 million steps at each potential interval from -200 to $+200$ mV. The error bars represent the standard deviation of three simulations per molecule. As the potential approaches the standard reduction potential E° , the probability of an oxidation reaction increases. (Bottom) At a scan rate of 5×10^3 V/s, the simulated voltammogram generated from the derivative of the probability curve with respect to time displays Nernstian behavior. Integration of the peak area yields 1.6×10^{-17} C, or 100 electrons, worth of current.

obtain $\Delta C_{\text{Red}}/\Delta t$ to generate a voltammogram (Figure 2, bottom). The scan rate associated with this voltammogram is 5×10^3 V/s. This scan rate is confirmed by integrating the anodic or cathodic peak area with respect to time. The calculated value is 1.6×10^{-17} C, which is equivalent to 100 electrons transferred via our 100, 1-electron process-simulated redox couples on the surface. Every molecule on the surface is converted from Red to Ox during the time scale of the voltammetric scan.

RESULTS AND DISCUSSION

Simulations of the random motion of a molecule confined in a hemispherical volume above an electrode provide a relatively simple model of the motion of a redox molecule tethered to an electrode surface via a flexible linker. This approximation can be viewed as such that the molecular tether causes the redox molecule to move with an apparent diffusion coefficient (D_{app}) that takes into account physical contributions of the tether. These contributions could arise from the polymer spring constant of the tether or electron hopping contributions for multiple redox centers.^{40,41} Regardless of what the factors are that affect the movement of the redox molecule, this movement can be expressed in terms of an apparent diffusion coefficient with units of square centimeters per second. Thus, the use of a

simple diffusion coefficient should effectively model the movement of a molecule about the surface of an electrode.

Encounters with the Electrode. The collisional frequency of the single molecule and the electrode surface is a function of both the tether length and the apparent diffusion coefficient. The collisional frequency ($A = \text{s}^{-1}$) was calculated by dividing the number of times the molecule hit the surface of the electrode (z position 0) during a simulation by the total simulation time. Shortening the tether distance from 20 to 5 nm or increasing the apparent diffusion coefficient from 10^{-5} to 10^{-3} cm^2/s dramatically increases the collision frequency between the molecule and surface (Figure 3). The data in

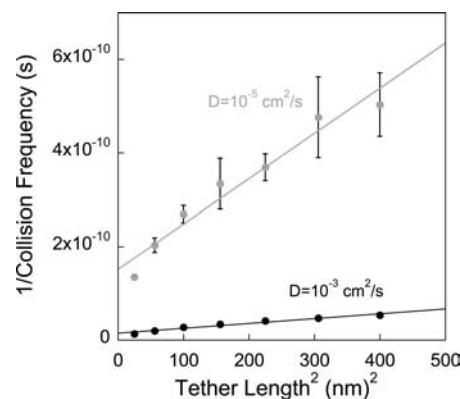


Figure 3. The collision frequency (number of collisions with the electrode surface per second) is a function of both the tether length and the diffusion coefficient of the molecule. Given the relationship of squared displacement ($L^2 = 6Dt$), the inverse of the collision frequency should be linear with respect to L^2 , with a slope of $1/6D$. Simulations run with both 10^{-5} and 10^{-3} cm^2/s diffusion coefficients exhibit this linear relationship, albeit at a less steep slope than the 1.67×10^4 and 167 s/cm^2 predicted, respectively, on account of nanoconfinement in the spherical volume. The slopes for simulations run with diffusion coefficients of 10^{-5} and 10^{-3} cm^2/s are 96 and 10 s/cm^2 , respectively. Error bars represent the standard deviation of at least 10, 10^7 -step simulations.

Figure 3 were obtained by simulating the random motion of a molecule for 10^7 steps. For a freely diffusing molecule with infinite boundaries, we expect the frequency to be linear with the inverse of the square tether length (L^2) through the relationship where net squared displacement is $L^2 = 6Dt$ (D is the diffusion coefficient (cm^2/s), and t is time (s)). Rearrangement of this expression should give a maximum collision frequency of $A = 6D/L^2$. As such, plotting the inverse of the collision frequency versus the square of the tether length should yield a line with a slope of $1/6D$.

The collision frequency at varying diffusion coefficients follows a linear relationship based on the square tether length L^2 (Figure 3), albeit with a lower slope than predicted above. This discrepancy is a result of the nanometer-scaled dimension of the spherical confinement. In addition, our molecule can reach its boundary at a z distance much shorter than the tether length as a result of the hemispherical geometry. The consequence of this nanoconfinement, in contrast to semi-infinite diffusion, is a higher collision frequency. As such, in a system with semi-infinite boundaries, a diffusion coefficient of 10^{-5} cm^2/s should yield a slope of 1.67×10^4 s/cm^2 , whereas our simulation yields a slope of 96 s/cm^2 .

Voltammetric Response of a Simulated Tethered Molecule. A randomly diffusing molecule, given enough

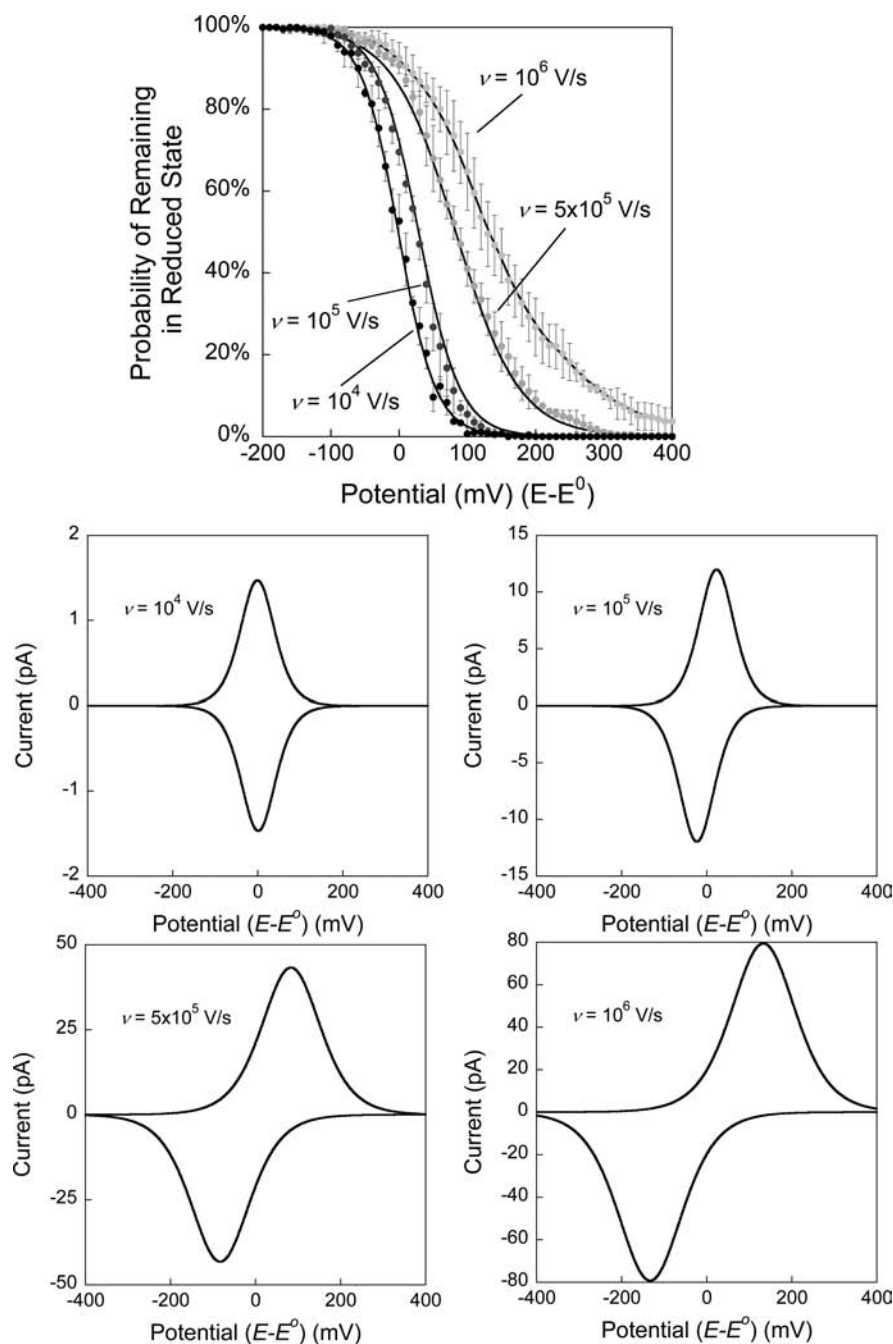


Figure 4. An increased voltammetric scan rate shifts the survival probability curves to more positive potentials and thus the voltammetric peaks further from E° . (Top) Survival probabilities of 100 molecules tethered via a 5 nm linker were simulated for various representative scan rates of 1×10^4 , 5×10^4 , 1×10^5 , 5×10^5 , and 1×10^6 V/s. Error bars represent the standard deviation of at least three simulations per molecule. (Bottom) The cyclic voltammograms, calculated from the shown probability curves, exhibit peak splitting and begin to look more like diffusion-limited voltammetry as the scan rate increases. Shown are the simulated voltammograms for the above scan rates.

time, has several opportunities to undergo an electron transfer event at any given applied potential. At large negative potentials ($E - E^\circ \leq -150$ mV) the probability of a reduction event occurring is overwhelmingly large compared to the probability of an oxidation event. As such, the molecule remains predominantly in the reduced state (Figure 2, top). The opposite is true at large positive potentials ($E - E^\circ \geq 150$ mV). At these positive potentials the oxidation reaction is favored, thus, it is likely that the molecule will be oxidized and remain in the oxidized state. Alternatively, when the applied potential is at the standard reduction potential, the probabilities of either

reaction are equal. While the highest absolute number of electron transfer events occurs at $E = E^\circ$, to observe the net current, the molecule must be converted from the reduced state and remain in the oxidized state.

At relatively long simulation time, and thus slower voltammetric scan rate (ν), a simulated voltammogram exhibits what appears to be surface-adsorbed or thin-layer-cell-type electrochemical behavior (Figure 2, bottom).³⁹ This manifests in the voltammogram as mirror image anodic and cathodic peaks with the same peak potentials as would be expected for an adsorbed Nernstian reaction.³⁹ As mentioned above, the

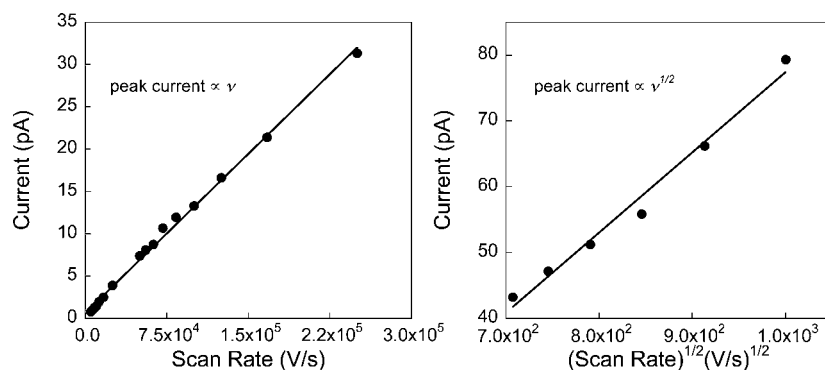


Figure 5. Voltammetric peak currents exhibit two voltammetric regimes corresponding to (left) surface-adsorbed and (right) diffusion-limited regimes. (Left) The peak currents from the cyclic voltammogram with different scan rates up to 2.5×10^5 V/s exhibit a linear dependence on the scan rate, indicative of surface-confined voltammetry ($y = 6.86 \times 10^{-1} + (1.26 \times 10^{-4})x$ ($R = 0.998$)). (Right) Conversely, at faster scan rates ($> 2.5 \times 10^5$ V/s), the peak current is proportional to the square root of the scan rate, indicative of a mass-transfer-limited electrochemical reaction ($y = 6.59 + (7.18 \times 10^{-5})x$ ($R = 0.997$)).

scan rate associated with this voltammogram is 5×10^3 V/s. At this scan rate the electrochemical reaction is not limited by the mass transfer of the redox molecule to the electrode surface.³⁹ The surface concentrations of the reduced and oxidized forms are thus in thermodynamic equilibrium with the applied potential. This type of electrochemical response is observed either when the redox molecule is adsorbed to the surface of the electrode or, in a thin-layer-cell setup, when the thickness of the electrochemical cell is much less than the thickness of the diffusion layer.³⁹ In both cases, the motion of the molecule is not important to the overall voltammetric response. In the simulation this thermodynamic control is observed because the molecule undergoes enough collisions with the electrode surface during the time scale of the experiment to successfully undergo electron transfer such that it is converted from the reduced state to the oxidized state.

While the relatively slow scan rate of 5×10^3 V/s exhibits voltammetric behavior indicative of an adsorbed species or thin-layer-cell-type response, the electrochemical response begins to change as the scan rate is increased (Figure 4). To increase the scan rate, the simulation is run using fewer steps, or for less time, at each potential increment. The consequence of fewer steps is that there are fewer collisions between the molecule and the electrode, leading to fewer opportunities for an electron transfer event to occur (Figure 4, top). This is seen as a shift in the survival probability plots to more positive potentials with increasing scan rates (Figure 4). For clarity, four representative scan rates are shown in Figure 4; however, the survival probability curves for all 20 simulated scan rates ranging from 1×10^6 to 5×10^3 V/s can be found in Figure S.1 in the Supporting Information. With fewer collisions between the molecule and electrode, a higher potential must be applied to ensure oxidation of the molecule. This is also seen by a shift in the peak potential in the simulated voltammograms (Figure 4, bottom). Voltammograms are calculated as indicated above by taking the derivative of the survival probability curves at 1 mV increments. Shown in Figure 4, bottom, are four representative voltammograms generated using the displayed probability curves (voltammograms from all 20 simulated scan rates can be found in the Figure S.1). Conway and co-workers observed a similar shift in peak potential when modeling the electrochemical response of an adsorbed species with no diffusion.⁴² In their study, however, the peak potential shift occurred at the onset of kinetic control, or as the electrochemical reaction

became irreversible. The scan rate at which this shift in potential occurs is seen in a plot of charge consumed during the reaction as a function of the scan rate. As the scan rate increased, they observed a decrease in charge as a result of the electron transfer rate limitation. An evaluation of the peak area as a function of the scan rate of our simulated data (Figure S.2, Supporting Information) shows that the charge is constant at 1.6×10^{-17} C except for the highest scan rate simulated. At a scan rate of 10^6 V/s, the charge consumed is less than what is required to oxidize all 100 molecules. Given this observation, the electrochemical reaction appears to be reversible at all scan rates $< 10^6$ V/s, and thus, we do not observe a kinetic limitation.

Evaluation of the voltammetric peak current as a function of the scan rate yields two distinct electrochemical behaviors of our simulated surface-confined molecule.³⁹ Analysis of our simulated peak currents as a function of the scan rate, using a 5 nm tether and 10^{-5} cm²/s diffusion coefficient, exhibits the behavior of a surface-confined reaction at slow scan rates and a diffusion-limited reaction at fast scan rates (see Figure 5 and Figure S.2 in the Supporting Information for a full plot of peak current vs scan rate). This observation is demonstrated at slower scan rates where the peak current is proportional to the scan rate (Figure 5, left), while at fast scan rates the peak current becomes linear with the square root of the scan rate (Figure 5, right). The former observation is indicative of a surface-confined reaction with no mobility of the redox molecule (peak current \propto scan rate (V/s)). Similarly, in thin-layer-cell electrochemistry, this proportionality is observed when the scan rate is slow compared to the diffusion time of the molecule of interest. Typically, this criterion is met when the layer thickness is much lower than the diffusion layer ($L \ll (2Dt)^{1/2}$, where t is the time of the voltammetric experiment).³⁹ Conversely, for a freely diffusing molecule (semi-infinite diffusion), the peak current follows Cottrell-like behavior and is proportional to the square root of the scan rate ($\nu^{1/2}$),³⁹ a result of the mass transfer limitation of the electrochemical reaction.

The two distinct regions of the voltammetric response of the simulated tethered redox molecule are a result of the experimental time scales relative to the predicted diffusion layer thickness, $(2Dt)^{1/2}$. For example, upon examining the 5 nm tether length voltammetry data, for the reaction to behave like an adsorbed species, the diffusion layer thickness must be 10-fold larger (50 nm) than the tether length, or $> 10L$. Using a

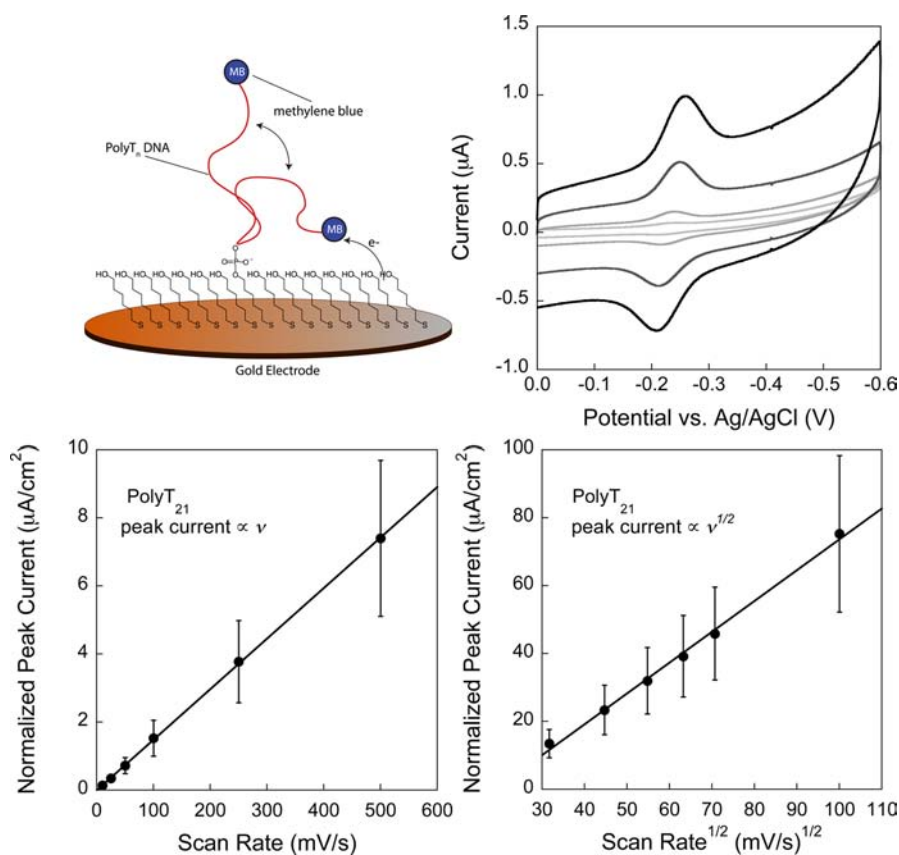


Figure 6. Methylene blue tethered to an electrode surface via a single-stranded DNA linker exhibits a voltammetric response in both the mass-transfer-independent and mass-transfer-limited regimes. (Top left) Experimental data were obtained with a monolayer of polyT₂₁ deposited on a gold electrode using (top right) cyclic voltammetry at various scan rates. (Bottom left) At slow scan rates (≤ 500 mV/s), the measured normalized peak currents are proportional to the scan rate ($y = (1.49 \times 10^{-8})x + (3.13 \times 10^{-9})(R = 0.999)$). (Bottom right) When using relatively fast scan rates, the voltammetric peak current is proportional to the square root of the scan rate ($y = (9.07 \times 10^{-7})x + (1.70 \times 10^{-5})(R = 0.996)$).

potential window of 600 mV (as is done in our simulations), this criterion is met at scan rates of $<4.8 \times 10^5$ V/s (see Figure 5). Conversely, when the predicted diffusion layer is $<10L$, the reaction becomes diffusion controlled. Using the $(2Dt)^{1/2} \geq 10L$ criterion, we calculate that, as the tether increases in length to 7.5, 10, 15, and 20 nm, the scan rates below which the reaction gives an adsorbed reactant electrochemical response are 2.13×10^5 , 1.2×10^5 , 5.3×10^4 , and 3×10^4 V/s, respectively. Intuitively, this trend is reasonable as the collision frequency decreases with increasing tether length; thus, there are fewer opportunities for electron transfer in the same time period (see Figure 2).

Voltammetric Response of DNA-Tethered Methylene Blue. The redox behavior of a redox-active methylene blue tethered to an electrode surface via a flexible DNA tether exhibits both a mass-transfer-limited regime and a mass-transfer-independent regime. That is, a transition from a diffusion-independent response at low scan rates to a diffusion-limited response at high scan rates is found by evaluating voltammetric peak currents (normalized to the electrode surface area, i_p/cm^2) at varying scan rate. Specifically, we investigated the electrochemical response, using cyclic voltammetry (Figure 6 and Figure S.3, Supporting Information), of gold electrodes modified with a mixed monolayer of polyT₂₁ DNA and a passivating mercaptohexanol layer.³³ The DNA strand is modified with a C₆-thiol at the 5'-end and with a methylene blue redox molecule at the 3'-end. Of note, methylene blue undergoes a two-electron, one-proton transfer

reaction, which is considerably more complicated than our one-electron transfer reaction used in our model.⁴³ Nonetheless, at lower scan rates (≤ 500 mV/s) the voltammetric peak current exhibits a linear proportionality to the scan rate (Figure 6, bottom left), while at the higher scan rates (>500 mV/s) the current is linearly proportional to the square root of the scan rate (Figure 6, bottom right). Similar behavior for DNA modified with ferrocene moieties has been observed by Anne and co-workers.¹ Because these transitions occur at voltammetric time scales where the electron transfer reaction is mass-transfer-limited, the nature of the electron transfer reaction does not affect the observation of these two regimes. This is further confirmed via the evaluation of the peak area, and thus charge, as a function of the scan rate (Figure S.4, Supporting Information), which remains relatively constant within error over the scan rates employed, indicating electrochemical reversibility. This trend, however, may not always hold true, for example, in cases of significantly high scan rate where the electron transfer reaction becomes rate limiting.

The transition from a diffusion-independent regime to a diffusion-limited regime depends on the length of the DNA tether. In addition to the polyT₂₁ DNA, we investigated modified electrode surfaces comprising polyT₁₄ or polyT₇ DNAs (Figure S.2, Supporting Information). Electrodes modified with these DNA strands also exhibit both diffusion-independent and diffusion-dependent behavior; however, the scan rates at which the transitions occur are different. While the polyT₂₁ shows a transition at scan rates >500 mV/s (or an

experimental time of 1.1 s considering our 550 mV potential window), polyT₁₄ and polyT₇ exhibit transitions at >1 and >4 V/s, respectively (equivalent to experimental times of 550 and 138 ms). This trend matches well, qualitatively, with what is predicted in our simulations. As the tether length is shortened, the collision frequency increases, which results in more opportunities for an electron transfer event to occur during the same amount of time.

The criterion set by our simulation of $(2Dt)^{1/2} \geq 10L$ can be used to estimate apparent diffusion coefficients (D_{app}) for the attached methylene blue. Using an estimated contour length for single-stranded DNA of $b_0 N_b$, where b_0 is the average distance between bases (6.3 Å) and N_b is the number of bases,⁴⁴ we calculate extended tether lengths of 4.4, 8.8, and 13.2 nm for polyT₇, polyT₁₄, and polyT₂₁, respectively. With these values of tether length and our criterion of $10L$, we estimate three very similar diffusion coefficients of 7.0×10^{-11} , 7.0×10^{-11} , and 7.9×10^{-11} cm²/s. These diffusion coefficients are slightly lower than those estimated by Anne and co-workers, who report a D_{app} of 7×10^{-10} cm²/s for a 20-nucleotide single-stranded DNA.¹ Alternatively, these values are slightly higher than those recently reported by Ferapontova and co-workers for methylene blue attached to double-stranded DNAs. They report, using cyclic voltammetry, an estimated diffusion coefficient of 1.72×10^{-11} cm²/s for a 16-nucleotide, double-stranded DNA.⁵

The slightly larger apparent diffusion coefficient measured by Anne and co-workers could be a result of the increased ionic strength employed during their electrochemical measurements. Specifically, in the experiments reported by Anne and co-workers, measurements were performed in a 1 M NaClO₄ solution compared to our 100 mM NaCl (with 25 mM tris(hydroxymethyl)aminomethane buffer). This increase in ionic strength lowers the persistence length of the DNA,⁴⁵ increasing the end-to-surface collision rate of the surface-bound DNA.⁴⁶ The consequence of this increase in collision rate is an increase in the apparent diffusion coefficient. Differences in the ionic strength could also contribute to differences in the apparent diffusion coefficients as a result of electrostatic interactions with the negatively charged backbone of the DNA. While we aim to minimize electrostatic contributions through the use of ionic strengths ≥ 100 mM,^{47,48} in our current experimental setup, we cannot eliminate them entirely. Finally, discrepancies may also arise on the basis of the surface density of DNAs used to perform the measurement. As the packing density increases, steric interactions between neighboring DNA strands become important^{8,31} in the transport of the redox molecule to the surface and could effectively reduce the apparent diffusion coefficient.

It may seem counterintuitive that methylene blue tethered to various lengths of DNA exhibits similar apparent diffusion coefficients, but it is important to consider the number of collisions the molecule undergoes with the electrode. As seen in our simulations (Figure 2), the collision frequency is a function of the tether length and diffusion coefficient. Ultimately, the current is a function of how many chances there are for an electron transfer event to occur, which is intimately linked to the tether length. The diffusion coefficient is the proportionality constant that relates the tether length to this collision frequency.

The observation of two voltammetric regimes has been previously observed in several flexible-tethered redox moieties. The aforementioned experiments by Amatore, Maisonhaute

and co-workers demonstrated that fullerodendrimers exhibit this behavior on account of the molecular linker tethering the C₆₀ moieties to the surface.²⁸ At sufficiently fast scan rates, the electrochemical response becomes limited by the flexibility of this linker. In studies of thin layers of polymerized vinyl-ferrocenes, Murray and co-workers²⁷ demonstrate that these flexible redox-active films exhibit electrochemical behavior indicative of both adsorbed and diffusion-limited responses. Furthermore, Anne and co-workers and Anne and Demaille have published several reports of ferrocene tethered to electrode surfaces with both single- and double-stranded DNAs with observed behavior similar to that described here.^{1,2} In these studies, the motion of the DNA is modeled using elastic bending. Nonetheless, the electrochemical response, both simulated and experimental, exhibits two distinct regimes. Much like the above-mentioned studies, we observe similar trends in surface-bound redox molecules with flexible linkers. Critical to these two regimes is the relationship of the experimental time scale, and thus diffusion layer, and the length of the molecular tether. When the diffusion layer thickness is $>10L$, the reaction is thermodynamically controlled. In other words, the reaction proceeds so rapidly that the population of redox moieties (in the reduced or oxidized state) is in thermodynamic equilibrium with the applied potential as described by the Nernst equation.²⁸ As the tether length becomes more appreciable compared to the diffusion layer, the reaction becomes diffusion controlled.

CONCLUSIONS

Using a simple single-molecule random walk simulation, we have simulated the electrochemical response of a redox molecule tethered to an electrode surface via a flexible linker. Our simulation predicts two regimes of electrochemical response—a regime with which the electrochemical response is not limited by mass transfer and thus behaves like an adsorbed redox molecule and a regime where the electrochemical response becomes diffusion limited.

Using a real example of a methylene blue attached to an electrode surface via a flexible DNA linker, we find this system exhibits electrochemical behavior similar to what is predicted by our simulations. The experimental time scales with which the two regimes occur are dependent on the number of nucleotides in the tethering DNA and thus the molecular tether length. From our experimental data, and using our new criterion of $(2Dt)^{1/2} > 10L$, we estimate reasonable apparent diffusion coefficients for the redox molecule attached to the electrode surface.

Changes in both the tether length and the apparent diffusion coefficient have been exploited in several oligonucleotide-based electrochemical sensors, including hybridization-based sensors^{4,9,30,31} and aptamer-based sensors.^{6,8,10,29} In either case the target binding event changes the apparent diffusion coefficient at which the appended redox molecule moves. This change can be a result of a single-stranded DNA with its complement^{26,31} or could be a result of an aptamer undergoing a conformation change to allow for target binding.^{8–10,29} Regardless of the interaction, the ultimate consequence is a change in the collision frequency of the molecule and the electrode surface. This manifests as a change in the measured peak current.

It should be noted that this is not the first model of an electrochemically active molecule tethered to an electrode surface via a DNA linker. Barton and co-workers describe the

electrochemical response of redox molecules tethered to an electrode surface where the density of the DNA precludes motion of the tether and thus electron transfer occurs through the DNA duplexes.⁴⁹ Anne and co-workers and Anne and Demaille have published several excellent reports on the electrochemical response of redox-modified DNA strands.^{1,26} To model the motion of DNA duplexes, they use an elastic diffusion model which allows the DNA duplex to bend; thus, their model incorporates physical contributions from the tether to the motion of the redox molecule.² Cheng and Makarov present a quantitative study of the reaction dynamics of a surface-attached biopolymer (DNA or polypeptide) using Langevin dynamics simulations.⁵⁰ Much like our model, at the end of the tether is an active molecule that can react with the surface. They derive quantitative expressions for reaction rates for a diffusion-controlled reaction, thus collision-rate-controlled, and a kinetically controlled reaction, controlled by the intrinsic kinetics of the distal molecule. While the model presented by Cheng and Makarov provides excellent information about the dynamics of the surface-attached polymer, their model does not take into consideration the time scale of the voltammetric experiments. Plaxco and co-workers also present a nice model of the motion of redox molecules tethered to an electrode surface.⁴⁶ In this paper, a coarse grain model of DNA flexibility defines the motion of the redox molecule. Using this model, they demonstrate the apparent electron transfer rate between a methylene blue and the electrode surface is determined by the equilibrium probability of the redox molecule approaching the surface and the electron transfer rate of the methylene blue through a passivating mercaptohexanol layer. Their model incorporates ionic strength and viscosity effects on these observed rates both experimentally and computationally. In addition, Plaxco and co-workers have demonstrated the effects of temperature and sequence on the end-to-end collisions of single-stranded DNA.⁵¹ All of these excellent models presented above utilize specific polymer physics to provide detailed information on the rates of reactions of distal-bound molecules. As such, these models provide realistic pictures of surface-confined redox molecules and allow for the incorporation of other contributing factors such as ionic strength, viscosity, and temperature. In our model, these factors would be incorporated through changes in the apparent diffusion coefficient describing the transport of the molecule to the surface.

Here, we develop a relatively simple, and generalized, model of a redox molecule tethered to an electrode via a flexible linker. In our model no intrinsic physics of the molecular tether are considered. Instead, we define the motion of the molecule using an apparent diffusion coefficient, which enables our model to be applied to a wide range of systems regardless of the type of diffusional motion. What dictates this diffusion coefficient will change on the basis of the tethering molecule. Regardless of what defines the motion of the molecule, the electrochemical response of such a system can be understood by comparing the diffusion layer thickness, and thus time scale of the voltammetric experiment, and the length of the tether. The apparent diffusion coefficient and tether length control the collision frequency (i.e., electron transfer opportunities) of the molecule and the electrode surface. In the event that the time scale of the experiment is slow such that the diffusion layer thickness $(2Dt)^{1/2}$ is 10 times the linker length, the electrochemical reaction will behave as an adsorbed molecule. At faster scan rates, and thus shorter diffusion layers, the reaction

becomes controlled by the motion of the attached redox molecule. Where this transition occurs can provide information about the apparent diffusion coefficient of the tethered molecule. We believe this simple approach will be of use in fields working with redox-active monolayers whether it is in the development of biosensors, molecular electronics, or smart materials.

■ ASSOCIATED CONTENT

📄 Supporting Information

Full plots of the peak current and peak area, both simulated and experimental, as a function of the scan rate and all simulated probability curves and resulting voltammograms. This material is available free of charge via the Internet at <http://pubs.acs.org>.

■ AUTHOR INFORMATION

Corresponding Author

rjwhite@umbc.edu

Notes

The authors declare no competing financial interest.

■ ACKNOWLEDGMENTS

We thank Dr. Bruce Johnson and Dr. Richard Wormsbecher for thoughtful discussions about simulation development and random walks.

■ REFERENCES

- (1) Anne, A.; Bouchardon, A.; Moiroux, J. *J. Am. Chem. Soc.* **2003**, *125*, 1112–1113.
- (2) Anne, A.; Demaille, C. *J. Am. Chem. Soc.* **2006**, *128*, 542–557.
- (3) Drummond, T. G.; Hill, M. G.; Barton, J. K. *Nat. Biotechnol.* **2003**, *21*, 1192–1199.
- (4) Fan, C.; Plaxco, K. W.; Heeger, A. J. *Proc. Natl. Acad. Sci. U.S.A.* **2003**, *100*, 9134–9137.
- (5) Farjami, E.; Campos, R.; Ferapontova, E. E. *Langmuir* **2012**, *28*, 16218–16226.
- (6) Ferapontova, E. E.; Olsen, E. M.; Gothelf, K. V. *J. Am. Chem. Soc.* **2008**, *130*, 4256–4258.
- (7) Kang, D.; Zuo, X.; Yang, R.; Xia, F.; Plaxco, K. W.; White, R. J. *Anal. Chem.* **2009**, *81*, 9109–9113.
- (8) White, R. J.; Phares, N.; Lubin, A. A.; Xiao, Y.; Plaxco, K. W. *Langmuir* **2008**, *24*, 10513–10518.
- (9) White, R. J.; Plaxco, K. W. *Anal. Chem.* **2009**, *82*, 73–76.
- (10) Willner, I.; Zayats, M. *Angew. Chem.* **2007**, *46*, 6408–6418.
- (11) Facchetti, A. *Chem. Mater.* **2010**, *23*, 733–758.
- (12) Wagner, M. *Angew. Chem.* **2006**, *45*, 5916–5918.
- (13) Bernhard, S.; Goldsmith, J. I.; Takada, K.; Abruña, H. D. *Inorg. Chem.* **2003**, *42*, 4389–4393.
- (14) Nyholm, L.; Nyström, G.; Mhramyan, A.; Strømme, M. *Adv. Mater.* **2011**, *23*, 3751–3769.
- (15) Yang, Y.; Wang, C.; Ashraf, S.; Wallace, G. G. *R. Soc. Chem. Adv.* **2013**, *3*, 5447–5452.
- (16) Levy, N.; Levi, M. D.; Aurbach, D.; Demadrille, R.; Pron, A. *J. Phys. Chem. C* **2010**, *114*, 16823–16831.
- (17) Brennan, B. J.; Liddell, P. A.; Moore, T. A.; Moore, A. L.; Gust, D. *J. Phys. Chem. B* **2012**, *117*, 426–432.
- (18) Yen, H.-J.; Chen, C.-J.; Liou, G.-S. *Adv. Func. Mater.* [Online early access]. DOI: 10.1002/adfm.201300569. Published Online: May 2, 2013. <http://onlinelibrary.wiley.com/doi/10.1002/adfm.201300569/full>.
- (19) Whittell, G. R.; Hager, M. D.; Schubert, U. S.; Manners, I. *Nat. Mater.* **2011**, *10*, 176–188.
- (20) Finklea, H. O.; Hanshew, D. D. *J. Am. Chem. Soc.* **1992**, *114*, 3173–3181.
- (21) Smalley, J. F.; Feldberg, S. W.; Chidsey, C. E. D.; Linford, M. R.; Newton, M. D.; Liu, Y.-P. *J. Phys. Chem.* **1995**, *99*, 13141–13149.

- (22) Murray, R. W. *Acc. Chem. Res.* **1980**, *13*, 135–141.
- (23) Longmire, M. L.; Watanabe, M.; Zhang, H.; Wooster, T. T.; Murray, R. W. *Anal. Chem.* **1990**, *62*, 747–752.
- (24) Anne, A.; Demaille, C.; Moiroux, J. *J. Am. Chem. Soc.* **2001**, *123*, 4817–4825.
- (25) Anne, A.; Demaille, C.; Moiroux, J. *Macromolecules* **2002**, *35*, 5578–5586.
- (26) Anne, A.; Demaille, C. *J. Am. Chem. Soc.* **2005**, *128*, 542–557.
- (27) Daum, P.; Lenhard, J. R.; Rolison, D.; Murray, R. W. *J. Am. Chem. Soc.* **1980**, *102*, 4649–4653.
- (28) Amatore, C.; Maisonhaute, E.; Nierengarten, J.-F.; Schöllhorn, B. *Isr. J. Chem.* **2008**, *48*, 203–214.
- (29) Radi, A.-E.; Acero Sánchez, J. L.; Baldrich, E.; O'Sullivan, C. K. *J. Am. Chem. Soc.* **2005**, *128*, 117–124.
- (30) Ikeda, R.; Kobayashi, S.; Chiba, J.; Inouye, M. *Chem.—Eur. J.* **2009**, *15*, 4822–4828.
- (31) Ricci, F.; Lai, R. Y.; Plaxco, K. W. *Chem. Commun.* **2007**, 3768–3770.
- (32) Yang, W.; Lai, R. Y. *Langmuir* **2011**, *27*, 14669–14677.
- (33) Xiao, Y.; Lai, R. Y.; Plaxco, K. W. *Nat. Protoc.* **2007**, *2*, 2875–2880.
- (34) Herne, T. M.; Tarlov, M. J. *J. Am. Chem. Soc.* **1997**, *119*, 8916–8920.
- (35) White, R. J.; White, H. S. *Anal. Chem.* **2005**, *77*, 214A–220A.
- (36) White, R. J.; White, H. S. *Langmuir* **2008**, *24*, 2850–2855.
- (37) Cutress, I. J.; Dickinson, E. J. F.; Compton, R. G. *J. Electroanal. Chem.* **2011**, *655*, 1–8.
- (38) Berg, H. C. *Random Walks in Biology*; Princeton University Press: Princeton, NJ, 1993.
- (39) Bard, A. J.; Faulkner, L. R. *Electrochemical Methods: Fundamentals and Applications*; Wiley: New York, 1980; Vol. 2.
- (40) Dill, K. A.; Bromberg, S. *Molecular Driving Forces: Statistical Thermodynamics in Chemistry and Biology*; Garland Science: New York, 2003.
- (41) Blauch, D. N.; Saveant, J. M. *J. Am. Chem. Soc.* **1992**, *114*, 3323–3332.
- (42) Angerstein-Kozłowska, H.; Klinger, J.; Conway, B. E. *J. Electroanal. Chem.* **1977**, *75*, 45–60.
- (43) Abi, A.; Ferapontova, E. E. *J. Am. Chem. Soc.* **2012**, *134*, 14499–14507.
- (44) Murphy, M. C.; Rasnik, I.; Cheng, W.; Lohman, T. M.; Ha, T. *Biophys. J.* **2004**, *86*, 2530–2537.
- (45) Chen, H.; Meisburger, S. P.; Pabit, S. A.; Sutton, J. L.; Webb, W. W.; Pollack, L. *Proc. Natl. Acad. Soc. U.S.A.* **2012**, *109*, 799–804.
- (46) Uzawa, T.; Cheng, R. R.; White, R. J.; Makarov, D. E.; Plaxco, K. W. *J. Am. Chem. Soc.* **2010**, *132*, 16120–16126.
- (47) Kaiser, W.; Rant, U. *J. Am. Chem. Soc.* **2010**, *132*, 7935–7945.
- (48) Rant, U.; Arinaga, K.; Fujita, S.; Yokoyama, N.; Abstreiter, G.; Tornow, M. *Nano Lett.* **2004**, *4*, 2441–2445.
- (49) Drummond, T. G.; Hill, M. G.; Barton, J. K. *J. Am. Chem. Soc.* **2004**, *126*, 15010–15011.
- (50) Cheng, R. R.; Makarov, D. E. *J. Phys. Chem. B* **2010**, *114*, 3321–3329.
- (51) Uzawa, T.; Isoshima, T.; Ito, Y.; Ishimori, K.; Makarov, D. E.; Plaxco, K. W. *Biophys. J.* **2013**, *104*, 2485–2492.